Check for updates

ChemCatChem

Research Article
doi.org/10.1002/cctc.202301677

Chemistry Europe
European Chemical Societies Publishing

www.chemcatchem.org

Anagostic Axial Interactions Inhibit Cross-Coupling Catalytic Activity in Square Planar Pyridinophane Nickel Complexes

Bailey S. Bouley,[a] Ian J. Garvey,[a] Hanah Na,[a, b] Ju Byeong Chae,[a] and Liviu M. Mirica*[a]

Herein, we report for the first time the use of the nitrogen-based bidentate molecule [2.2]pyridinophane (N2) as a ligand for metal complexes. Additionally, its improved synthesis allows for electronic modification of the pyridine rings to access the new *para*-dimethylamino-[2.2]pyridinophane ligand (*p*-NMe_2N2). These ligands bind nickel in an analogous fashion to other pyridinophane ligands, completing the series of tetra-, tri-, and bidentate pyridinophane-nickel complexes. The new compounds exhibit geometrically enforced C–H anagostic interactions between the ethylene bridge protons and the nickel center that are not present in other pyridinophane systems. These ethylene bridge groups also act as an unusual form of steric encumbrance, enforcing square planar geometries in ligand fields that would otherwise adopt tetrahedral structures. In addition, these anagostic interactions inhibit the catalytic performance in Csp^3–Csp^3 Kumada cross coupling reactions relative to other common bidentate N-ligand platforms, possibly by preventing the formation of the 5-coordinate oxidative addition intermediates.

1. Introduction

The evaluation of Ni-based transformations as a potential earth-abundant substitute for palladium has recently gained notable popularity, especially in the realm of C–C and C–X cross coupling reactions.[1] However, divergent reactivity between nickel and palladium catalysts has complicated attempts to directly translate these transformations between metal centers. The propensity of Ni to undergo single electron transfer (SET) reactions makes mechanistic insight challenging in most cases. However, there are some intrinsic properties of Ni catalysis that make it the more attractive option in some reactions over palladium. For example, the lower *d* orbital diffusivity of Ni ions is hypothesized to make β-hydrogen elimination less favorable, thus making it more suitable for sp^3–sp^3 cross couplings.[2] More recently, Ni-based photocatalysis as a means to access new reactivity, especially in the realm of C–O cross coupling, has gained significant traction in the literature.[3] Some of these Ni catalysts, when used in the absence of an auxiliary photocatalyst, typically bear a photo-labile halide or aryl group, which initiates reactivity in a I–III–I catalytic dark cycle from a Ni(II) precatalyst.[4]

Among Ni-catalyzed reactions, something frequently observed is the use of nitrogen-based bidentate ligands, such as bipyridine, phenanthroline, or bis(oxazoline) ligands, in order to facilitate oxidative addition/reductive elimination from the ill-characterized Ni(I) and Ni(III) oxidation states.[5] Our understanding of these electronic configurations is limited, owing to their highly reactive nature. One of the methods our group has previously utilized to study reactivity from these oxidation states is through the use of flexible, multidentate ligands such as pyridinophane macrocycles.[6] These ligands are able to undergo conformational changes,[7] providing denticity as needed to improve stability of higher oxidation states for study. Though we have studied extensively tetradentate pyridinophane scaffolds,[8] and more recently, the tridentate analogue,[4c] the use of the bidentate pyridinophane [2.2]pyridinophane (N2) as a ligand for metal complexes has not been reported to date, although it was initially synthesized by Inazu et al. in 1988.[9] Translating the reactivity of high-valent Ni from these tri- and tetradentate N-donor ligands to the more catalytically relevant bidentate N-donor ligands has been a challenge, and we considered that the use of the bidentate macrocycle N2 may allow for a better understanding of reactivity differences between these ligand classes (Figure 1).

2. Preparation of Nickel Complexes

The new synthesis of the bidentate pyridinophane ligand N2 (**L1**) involves skeletal editing of the common pyridinophane precursor (^{H}N4, see Supporting Information for details).[10] Though **L1** has been shown crystallographically to adopt a "chair" conformation in the solid state, binding to metal ions

[a] B. S. Bouley, I. J. Garvey, Dr. H. Na, J. Byeong Chae, Prof. L. M. Mirica
Department of Chemistry, University of Illinois Urbana-Champaign, 505 S Mathews Ave, Urbana, IL 61801, USA
E-mail: mirica@illinois.edu

[b] Dr. H. Na
Center for Advanced Specialty Chemicals, Korea Research Institute of Chemical Technology (KRICT), Ulsan 44412, Republic of Korea

Supporting information for this article is available on the WWW under https://doi.org/10.1002/cctc.202301677

© 2024 The Authors. ChemCatChem published by Wiley-VCH GmbH. This is an open access article under the terms of the Creative Commons Attribution Non-Commercial NoDerivs License, which permits use and distribution in any medium, provided the original work is properly cited, the use is non-commercial and no modifications or adaptations are made.

© 2024 The Authors. ChemCatChem published by Wiley-VCH GmbH

Research Article
doi.org/10.1002/cctc.202301677
Chemistry Europe
European Chemical Societies Publishing

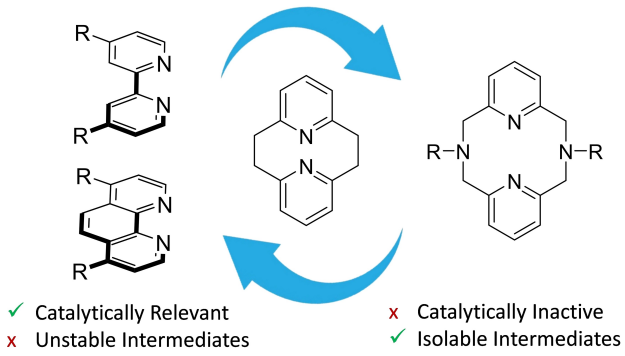

Figure 1. Relationship between catalytically relevant N-donor ligands (left) and pyridinophane macrocycles used to characterize unstable intermediates (right) in Ni-mediated Kumada cross-coupling reactions.

results in a rearrangement into a "boat" conformation, allowing for a *cis*-coordinated bis-nitrogen ligand environment (Figure 2). This structural rearrangement occurs spontaneously in solution, as ^{1}H NMR resonances for the ethylene protons are split and exhibit broadening, indicating a dynamic conformational behavior at room temperature (Figure S1). To demonstrate that **L1** could support a variety of Ni complexes with varying ligand field environments, the *cis*-dichloride Ni complex (**1**) and the organometallic complexes N2Ni(*o*-tolyl)Cl (**3**) and N2Ni(*p*-tolyl)Cl (**4**) were synthesized (Figure 2). We viewed that the N2 ligand framework could provide a comparison between the non-conjugated pyridinophane frameworks, for which reactive species can be isolated and characterized, and the more catalytically relevant conjugated bipyridyl (bpy) frameworks. The attention the bpyNiX$_2$ and bpyNi(aryl)Cl catalysts have received in the realm of photocatalyzed cross couplings sparked our initial interest in studying the pyridinophane analogues of these systems. Two issues that we observed with **L1** were the relatively low solubility of the complexes, as well as their propensity to be displaced by coordinating solvents. The crystallographic extended structures for these compounds show very tight molecular packing, which may contribute to their decreased solubility. Furthermore, though ligand lability may be a desired characteristic in some catalytic systems, this is not the case for studying the intrinsic properties of these frameworks. To rectify these issues, the strongly electron-donating *para*-dimethylamino-N2 (*p*–NMe$_2$N2, **L2**) was synthesized using a procedure analogous to that used for **L1** (see Supporting Information). The increased electron-donating ability of **L2** addresses both issues, increasing the solubility of the complexes in polar solvents, as well as decreasing the ligand lability. This new synthetic route opens up new methods to functionalized macrocyclic *p*–X–^{R}N4, *p*–X–^{R}N3, and *p*-X–N2 ligands, which we hope to explore in more detail in the near future.

3. Analysis of Anagostic Interactions

Complexes **1**–**6** were all crystallographically characterized, revealing some unexpected properties of these complexes that were worth investigating: the ethylene –CH$_2$CH$_2$– bridges between the pyridine rings were situated directly over the axial positions of the metal centers which may have some form of interaction; in addition, the dichloride complexes **1** and **2** adopt a square planar geometry (τ_4' = 0.13 and 0.11,[11] torsion angle = 3.5° and 1.9°, respectively). These τ_4' values are similar to those observed for complexes **3**–**6** (τ_4' = 0.11, 0.15, 0.10, and 0.13,

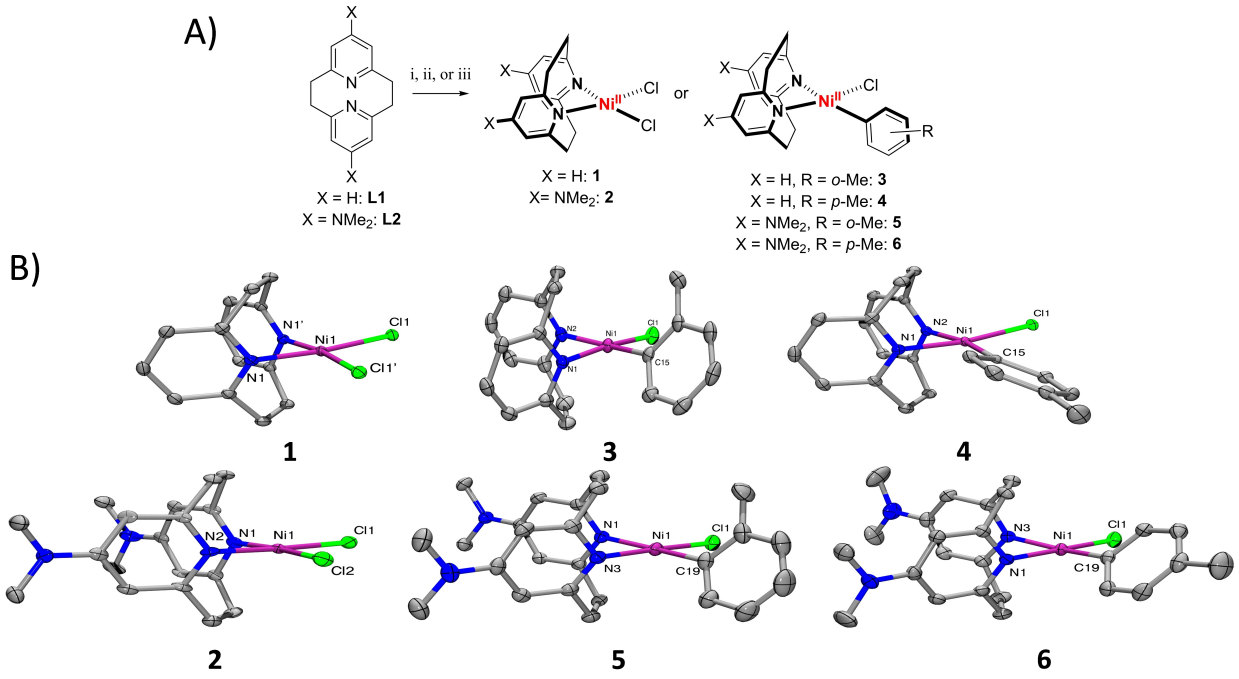

Figure 2. A) Synthesis of metal complexes i) (DME)NiCl$_2$, CH$_2$Cl$_2$, RT; ii) Ni(COD)$_2$, 2-ClPhMe, RT; iii) Ni(COD)$_2$, 4-ClPhMe, RT. See Supporting information for additional details. B) ORTEP representations of complexes **1**–**6**. Ellipsoids shown at 50% probability.

© 2024 The Authors. ChemCatChem published by Wiley-VCH GmbH

18673899, 2024, 5, Downloaded from https://chemistry-europe.onlinelibrary.wiley.com/doi/10.1002/cctc.202301677 by University Of Illinois At, Wiley Online Library on [30/07/2024]. See the Terms and Conditions (https://onlinelibrary.wiley.com/terms-and-conditions) on Wiley Online Library for rules of use; OA articles are governed by the applicable Creative Commons License

respectively). Dihalide Ni complexes supported by bidentate nitrogen ligands usually exhibit tetrahedral geometries with magnetic moments indicative of triplet electronic states in solution.[12] *Cis*-dihalide Ni complexes with square planar geometry typically require stronger-field ligands such as bidentate phosphines, or N-based ligands that carry extreme steric bulk.[13] In order to rationalize this discrepancy, we hypothesized that the close proximity of the C–H bonds from the ethylene bridges to the Ni center provides a unique form of steric bulk enforcing the planar geometry. Steric control through C–H bonds is counter-intuitive, since it is the smallest organic functional group possible, and as such, this property is unique to these ligand platforms and merit further interrogation. Buried volume ($\%V_{bur}$) calculations[14] show that **L1** has a buried volume of 51.3%, with 11.2% coming directly from the ethylene groups (Figure 3 and Table S22). This observed buried volume is larger than is typical for bidentate nitrogen ligand systems such as bipyridine ($\%V_{bur} = 35.7\%$) or TMEDA ($\%V_{bur} = 46.2\%$) and is similar to the buried volume of the extremely bulky diisopropylphenyl-substituted β-ketoimine ligand (Dipp-NacNac, $\%V_{bur} = 52.9\%$), which despite its steric bulk, still allows for a tetrahedral geometry in its Ni dichloride complex.[14]

The geometric information for the relationship between the Ni centers and the proximal C–H bonds for complexes **1**–**6** are shown in Table 1 and represented visually in Figure 4. The data initially appear conflicting. The Ni–H bond distances are in the ~2.7–2.8 Å range, indicative of an anagostic interaction,[15] yet the Ni–H–C bond angles are close to 90° in most cases, which is more indicative of an agostic-type interaction.[16] To resolve the discrepancy, ^{1}H NMR experiments and density functional theory (DFT) computational studies were performed to further analyze the nature of the Ni···H–C interaction in these complexes.

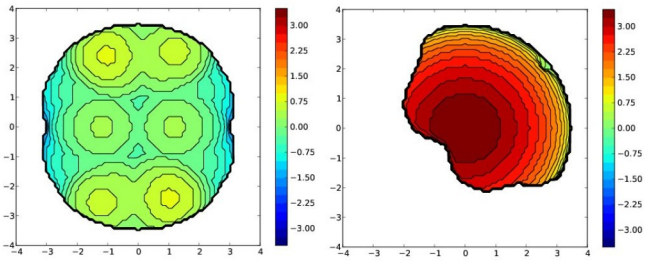

Figure 3. Calculated buried volume ($\%V_{bur}$) for **L1**, shown from a face-on orientation (left) and from a top-down orientation (right).

Complexes **2**–**6** were all characterized by ^{1}H NMR in CD_2Cl_2, all of which showed diamagnetic behavior, although the spectrum of **2** was slightly paramagnetically broadened ($\mu_{eff} = 1.4\ \mu_B$). We can rule out that this paramagnetic behaviour is due to an inherent geometric distortion, since the geometric index τ_4' for **2** is similar to those of the aryl chloride complexes **3**–**6**. Unfortunately, due to the insolubility of **1** in common NMR solvents, we were not able to analyze the complex in this manner. Nevertheless, we were able to obtain solid-state SQUID data for this complex to probe its paramagnetism in the solid state (Figure S35). However, the crystal packing of **1** indicates a very short intermolecular Ni–Ni distance of 6.7 Å, which could lead to long-range ferromagnetic ordering, affecting these solid-state measurements. Analysis of the magnetism of **1** in the solid state gives a $\mu_{eff} = 2.31\ \mu_B$ near room temperature, which, like the Evans' method data for **2**, suggests some degree of paramagnetic behavior. We attribute the partial observed paramagnetism to some degree of conformational flexibility of the complex between a planar singlet state and a triplet twisted state that interconvert in solution (see below). The ^{1}H NMR signals for complexes **2**–**6** show a splitting of the ethylene protons, with half of the resonances moving to extremely downfield ppm chemical shifts (~3.5 ppm vs. those of the free ligand), while the other half resonances remaining in a similar range to the free ligand with a slight downfield shift (~0.9 ppm). We attribute these signals to the ethylene protons located proximally to the Ni center (referred to as "anagostic") and those oriented away from the Ni center respectively (referred to as "geminal", Table 1). This large downfield shift is consistent with a significant anagostic interaction. These ^{1}H NMR results in conjunction with the crystallographic Ni–H bond distances suggests anagostic behavior with an unusually acute Ni–H–C bond angle.

To further validate these anagostic interactions, DFT calculations were performed at the PBE1PBE/def2-TZVP level of theory to analyze the nature of these bonds as well as the orbital interactions between the Ni center and the C–H bonds. To this end, natural bonding orbital (NBO) analysis was conducted to determine the Wiberg bond order of the individual C–H bonds (Table 1). All complexes show a marked decrease in bond order for the C–H bonds axial to the Ni center

Table 1. C–H bond data for ethylene protons for complexes **1**–**6**.

Complex	Ni–H bond distance ($Å_{avg}$)	NiH–C bond angle ($°_{avg}$)	^{1}H chemical shift vs free ligand[a] (anagostic, geminal, Δppm)	$Calc_{avg}$ Wiberg C–H bond order (anagostic, geminal)
1	2.765	89.3	–	0.9075, 0.9234
2	2.787	88.9	+3.98, +0.99	0.8943, 0.9138
3	2.783	89.7	+3.42, +0.90	0.9035, 0.9121
4	2.756	90.4	+3.28, +0.87	0.8930, 0.9127
5	2.809	89.9	+3.36, +0.76	0.8962, 0.9148
6	2.788	90.0	+3.22, +0.73	0.8964, 0.9152

[a] ^{1}H NMR data collected in CD_2Cl_2. Free ligand chemical shift determined by the numerical average of the two singlets corresponding to the bridging ethylene proton signals.

© 2024 The Authors. ChemCatChem published by Wiley-VCH GmbH

18673899, 2024, 5, Downloaded from https://chemistry-europe.onlinelibrary.wiley.com/doi/10.1002/cctc.202301677 by University Of Illinois At, Wiley Online Library on [30/07/2024]. See the Terms and Conditions (https://onlinelibrary.wiley.com/terms-and-conditions) on Wiley Online Library for rules of use; OA articles are governed by the applicable Creative Commons License

Research Article
doi.org/10.1002/cctc.202301677
Chemistry Europe
European Chemical Societies Publishing

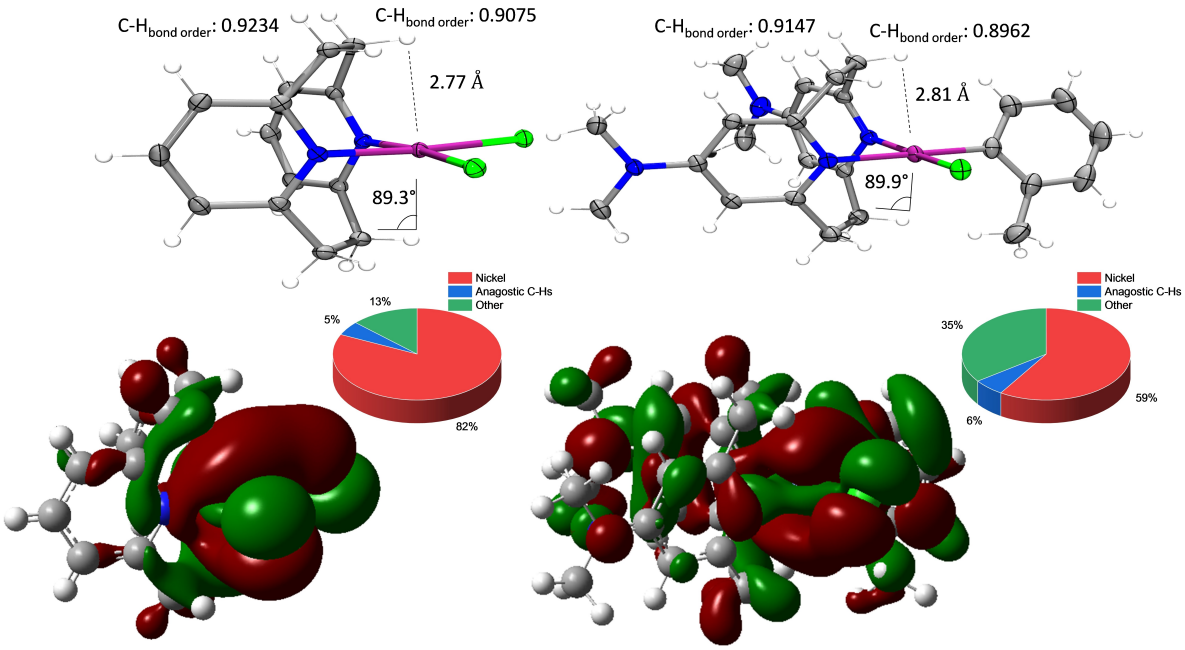

Figure 4. ORTEP representations of **1** (top left) and **5** (top right), with labels for relevant anagostic Ni···H–C interactions. Representative MOs of **1** (HOMO−1, bottom left) and **5** (HOMO, bottom right), showing repulsive interactions between Ni d_{z^2} orbitals (shown at a 0.01 isovalue) and ethylene C–H bonds. Included pie charts for each complex show atomic orbital contributions from the relevant atom groups.

relative to geminal C–H bonds, with differences ranging from −0.0090 to −0.0193 (Table 1 & Figure 4). This decrease in C–H bond order is consistent with literature reports of anagostic interactions in Ni(II) complexes.[17] Furthermore, the MO compositions of complexes **1**–**6** were generated to visualize possible Ni center electrostatic interactions with the ethylene protons. Since an anagostic interaction may be repulsive in nature between the occupied metal *d* orbitals and the C–H bonds, it is expected that a high energy occupied orbital should contain an repulsive interaction between the Ni d_{z^2} orbital and the C–H bond due to their close proximity and the geometry around the metal center.[18] Gratifyingly, all complexes show such an MO interaction in at least one of the frontier MOs (Tables S23 and S24). Altogether, the experimental results, in tandem with the calculated parameters, indicate that Ni complexes supported by the bidentate pyridinophane N2 scaffold bear strong anagostic interactions with the axially situated C–H bonds of the bridging ethylene groups and an unusually acute Ni–H–C bond angle, which is enforced by the constrained ligand geometry.

Finally, to better understand the steric effects of these ethylene groups, square planar singlet ground states and the corresponding tetrahedral triplet ground states were independently optimized via DFT calculations. Both dichloride complexes **1** and **2** show no significant thermodynamic preference for square planar over tetrahedral geometries (Figure 5). Calculation of the expected equilibrium constant between these two singlet and triplet states leads to an expected magnetic moment of of 1.36 or 1.60 μ_B for **1** and **2**, respectively, which is in good agreement with the experimental values obtained for **1** and **2**, and thus benchmarking the computational results. As expected for Ni(II) organometallic compounds, the thermodynamic preference for the square planar geometry for complexes **3**–**6** is clear, with ΔG values between +6.9 and +9.4 kcal/mol. The sharp ^{1}H NMR signals suggest a singlet square planar d^8 electronic state, and the strong σ-donating ability of organometallic ligands on Ni(II) centers are known to enforce square planarity.[4a,6d,19] All optimized triplet geometries demonstrate a distortion of the ethylene bridges between the pyridine rings to accommodate for the new orientation of the auxiliary ligands,

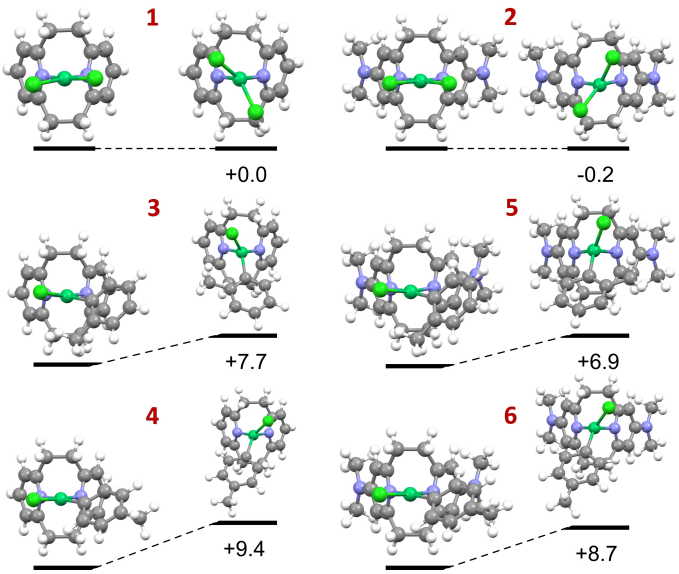

Figure 5. Energy diagrams for the DFT optimized conversion of square planar singlet structures to tetrahedral triplet structures for complexes **1**–**6**. Energies shown in kcal/mol.

© 2024 The Authors. ChemCatChem published by Wiley-VCH GmbH

18673899, 2024, 5, Downloaded from https://chemistry-europe.onlinelibrary.wiley.com/doi/10.1002/cctc.202301677 by University Of Illinois At, Wiley Online Library on [30/07/2024]. See the Terms and Conditions (https://onlinelibrary.wiley.com/terms-and-conditions) on Wiley Online Library for rules of use; OA articles are governed by the applicable Creative Commons License

as well as fairly low torsion angles for tetrahedral structures (36°–45°). These data implicate that given the unique structure of the N2 ligand framework, a strong steric clash exists between the ethylene bridge C–H groups and the chlorides/aryl groups, preventing the formation of a fully tetrahedral geometry.

4. Kumada Cross-Coupling Catalysis

One area we had interest in exploring with this new class of molecules were cross-coupling reactions, especially in comparing their effectiveness to other common bidentate and tridentate ligand scaffolds. Ni-mediated Csp^3–Csp^3 cross-couplings are particularly notable, as higher thermodynamic barriers to β-hydride elimination relative to Pd-based systems may improve catalytic stability and decrease unwanted side reactions.[20] One common mechanism for cross-coupling reactions using Ni(II) catalysts involves the generation of a Ni(I) intermediate that undergoes oxidative addition (either concerted or *via* a single-electron transfer pathway, Figure 6A) to generate a Ni(III) species, followed by transmetalation, and then reductive elimination to regenerate the active Ni(I) species.[21] Furthermore, depending on the identity of the X ligand in the Ni(I) species, transmetalation may occur prior to oxidative addition.[22] We have recently reported a Ni dichloride catalyst supported by a 1,4,7-triisopropyl-1,4,7-triazacyclononane (iPr_3TACN) ligand which is an efficient catalyst for the alkyl–alkyl Kumada cross-coupling reaction, and we were interested in probing the catalytic reactivity of the bidentate Ni(II) complexes reported herein.[23] In our previous study, it was found that the addition of acetonitrile to the reaction improved the cross-coupled product yields, likely by providing additional stability to the active Ni(I) catalyst, facilitating productive reductive elimination from the Ni(III) state, and disfavoring β-hydride elimination leading to generation of alkene side products and catalytic deactivation. Employing these optimized reaction conditions, we have performed alkyl–alkyl Kumada cross-coupling reactions for complexes **1**–**6** and related Ni complexes (Figure 6B).

Among complexes **1**–**6**, only complexes **1**–**4** gave appreciable amounts of alkyl–alkyl cross-coupled product. The differences between the dichloride complexes and the aryl halide complexes supported by **L2** may suggest that the presence of the strongly σ-donating aryl group and a stronger electron-donating ligand may contribute to the instability of the generated Ni(I) complex. The notable enhanced catalytic activity of the 4,4′-di-tert-butyl-2,2′-bipyridyl (dttbpy) and (iPr_3TACN)Ni dichloride complexes over **1** and **2** is likely due to the ability of these common ligands to provide a sweet spot between stability and reactivity of the Ni(I) and/or Ni(III) states in order to avoid catalyst decomposition. One interesting comparison is the relative reactivity between the aryl halides supported by **L1** and **L2** and those supported by dttbpy. In the case of dttbpy, the aryl halide complex gives a yield improvement over the dichloride, while the opposite trend was observed for the N2 ligands. We postulate that this inversion is related to the relative geometries of these complexes. In the case of complexes **1**–**6**, all exhibit square planar geometries, suggesting reactivity differences solely arise from stability of the generated Ni(I) intermediates. By comparison, (dttbpy)$NiCl_2$ exhibits a tetrahedral geometry, while (dttbpy)Ni(*o*-tolyl)Cl exhibits a square planar geometry similar to the (*p*–XN2)Ni complexes. Therefore, one possible explanation for the decreased catalytic competence could be the result of the necessary geometric rearrangement to adopt a more planar geometry preferred by the Ni(I) intermediates. A similar role for the planar geometry of the Ni catalysts was previously reported for ethylene polymerization reactions.[24]

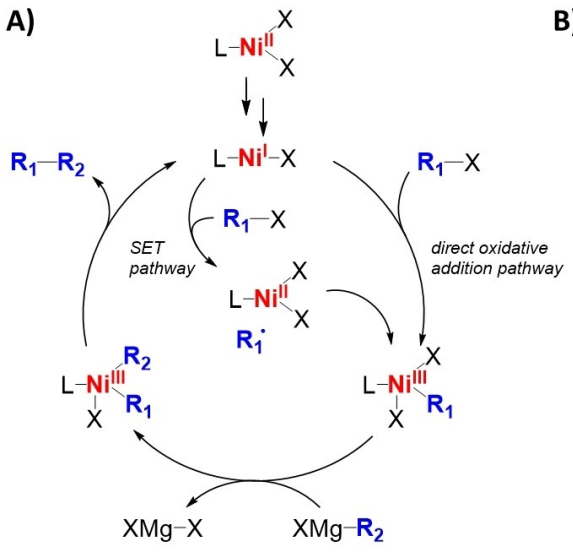

B)

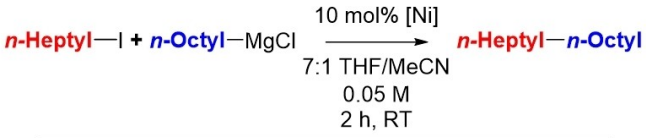

[Ni]	Yield (%)[a]
1	**14**
2	**11**
3	**11**
4	**11**
5	**6**
6	**1**
dttbpyNiCl$_2$	**41**
dttbpyNi(*o*-tolyl)Cl	**46**
iPr$_3$TACNNiCl$_2$	**66**
DME(Ni)Cl$_2$	**7**
L1 or L2 only	**0**

Figure 6. A) Proposed catalytic cycle for the Ni-mediated Csp^3–Csp^3 Kumada cross-coupling reaction. B) alkyl–alkyl Kumada cross coupling yields for complexes **1**–**6** and related Ni complexes under previously optimized conditions. [a] Yields were obtained by GC–FID and were corrected with calibration curves using dodecane as an internal standard (See supporting information for experimental details).

© 2024 The Authors. ChemCatChem published by Wiley-VCH GmbH

18673899, 2024, 5, Downloaded from https://chemistry-europe.onlinelibrary.wiley.com/doi/10.1002/cctc.202301677 by University Of Illinois At, Wiley Online Library on [30/07/2024]. See the Terms and Conditions (https://onlinelibrary.wiley.com/terms-and-conditions) on Wiley Online Library for rules of use; OA articles are governed by the applicable Creative Commons License

18673899, 2024, 5, Downloaded from https://chemistry-europe.onlinelibrary.wiley.com/doi/10.1002/cctc.202301677 by University Of Illinois At, Wiley Online Library on [30/07/2024]. See the Terms and Conditions (https://onlinelibrary.wiley.com/terms-and-conditions) on Wiley Online Library for rules of use; OA articles are governed by the applicable Creative Commons License

The overall reactivity differences between the bidentate ligands **L1/L2** and dttbpy is worth further discussion. The most obvious structural difference is the axial ligation potential, which is absent in the bidentate pyridinophane ligands, but present in the bipyridyl-based ligands. Ni(I)/Ni(III)/Ni(I) catalytic cycles supported by bidentate ligands typically undergo oxidative addition from a three- to a five-coordinate geometry, which necessitates axial ligation to generate either a square pyramidal or trigonal bipyramidal geometry.[25] Therefore, the inability of (N2)Ni and (*p*–NMe_2N2)Ni complexes to undergo oxidative addition may be prohibiting productive cross-coupling. This can be observed in the GC-FID data for the catalytic reactions, in which complexes **1**–**6** generate ~1 equiv. heptane relative to the Ni catalyst, suggesting that the initial iodide abstraction to generate the alkyl radical is not followed by a rebound step, and instead hydrogen atom abstraction from either THF or adventitious water yields the alkane side product (Table S1). Other possibilities for inhibited reactivity may be due to a change in coordination number of the N2-type ligands from κ^2 to κ^1 that may have unintended steric consequences. While there is no evidence of isomerization at the Ni(II) state due to the lack of fluxionality observed in the ^{1}H NMR spectra of complexes **3**–**6**, the ligand flexibility at the Ni(I) state cannot be completely excluded, though 2-coordinate LX–Ni(I) complexes are less likely to be stable. These results support the assignment of catalytic inhibition due to the anagostic C–H bonds in (N2)Ni and (*p*–NMe_2N2)Ni complexes and emphasize the importance of stabilizing the odd-oxidation state Ni intermediates in order to allow for efficient alkyl–alkyl cross-coupling reactions.

5. Conclusions

We have demonstrated for the first time that the smallest pyridinophane, [2.2]pyridinophane (N2), is capable of coordinating to metal ions in a comparable manner to the higher-denticity tridentate and tetradentate pyridinophanes. We have also synthesized for the first time electron-rich pyridinophanes bearing *para*-dimethylamino functional groups. In the process of studying the coordination chemistry of these platforms, we discovered unintended steric contributions from the ethylene bridge C–H bonds situated in close proximity to the Ni center, an extremely unique form of steric encumbrance caused by the smallest functional group. These geometrically enforced Ni–C–H interactions are best described as anagostic interactions, as shown by NMR and x-ray crystallography, and supported by DFT calculations. Furthermore, we have demonstrated that these sterically encumbering C–H bonds inhibit catalytic performance in Csp^3–Csp^3 primary alkyl–alkyl cross-couplings, likely by preventing the formation of the five-coordinate Ni(III) intermediate after oxidative addition. Furthermore, the more electron-donating capabilities of **L2** may be contributing to further reduced stability of the Ni(I) state. These results indicate that a ligand design which only stabilizes Ni(III) and Ni(I) intermediates may not be sufficient for productive reactivity, and that sufficiently accessible coordination sites are necessary for catalytic turnover.

Experimental Section

Synthesis of L1[9] **and L2**. One equiv. ^{H}N4 or *p*–$NMe_2{}^H$N4 were dissolved in concentrated HCl to make an approximately 0.1 M solution. Separately, 9.4 equiv. $NaNO_2$ was dissolved in an equal volume of cold H_2O. The $NaNO_2$ solution was added to the HCl solution dropwise open to air to allow the venting of NO_2 gas. The reaction was stirred for 16 hours at room temperature, after which the reaction was basified to pH 14 using 4 M KOH. The reaction was then diluted with an equal volume of 200 proof EtOH and heated to reflux under a nitrogen atmosphere for 1 hour after which 5.4 equiv. sodium dithionite was added. The reaction solution was allowed to reflux under N_2 for an additional 3 hours, after which the solution was cooled to room temperature, diluted with 30 mL DI water, and extracted into 3×100 mL CH_2Cl_2. The organic layer was dried, filtered, and concentrated via rotary evaporation. The crude solid was washed with a small volume of MeCN to give **L1** or **L2** as white solids (See SI for full characterization data). NMR data for **L1**: ^{1}H NMR (600 MHz, $CDCl_3$) δ 7.60 (t, J = 7.5 Hz, 2H), 7.10 (d, J = 7.5 Hz, 4H), 3.24 (br, 4H), 2.55 (br, 4H); ^{13}C NMR (151 MHz, $CDCl_3$) δ 160.05, 137.43, 119.73, 40.33. NMR data for **L2**: ^{1}H NMR (600 MHz, $CDCl_3$) δ 6.35 (s, 4H), 3.05 (d, J = 7.7 Hz, 4H), 2.98 (s, 12H), 2.51 (d, J = 7.8 Hz, 4H); ^{13}C NMR (151 MHz, $CDCl_3$) δ 160.91, 155.85, 102.97, 41.22, 39.28.

Synthesis of 1. In a glovebox, 30 mg of **L1** (1 equiv) was suspended alongside 31.4 mg of (DME)$NiCl_2$ (1 equiv) in 10 mL dichloromethane. The solution was allowed to stir for 16 hours, during which the solution turned from yellow to dark purple. The resulting suspension was filtered, and the purple solid was washed with CH_2Cl_2, followed by THF, then diethyl ether. The purple powder was dried under vacuum to give 35 mg of the product as a dark purple powder in 73% yield. X-ray quality crystals were obtained from layering a THF solution of (DME)$NiCl_2$ onto a CH_2Cl_2 solution of **L1** at room temperature (See SI for full characterization data).

Synthesis of 2. In a glovebox, 30 mg of **L2** (1 equiv) was suspended alongside 22.1 mg of (DME)$NiCl_2$ (1 equiv) in 10 mL dichloromethane. The solution was allowed to stir for 16 hours, during which the solution turned from yellow to dark blue. The resulting solution was filtered, and the crude product was precipitated with pentane. The precipitate was filtered and washed with diethyl ether and pentane and dried under vacuum to give 21 mg of the product in 49% yield as a blue powder. X-ray quality crystals were obtained from slow diffusion of pentane into a CH_2Cl_2 solution of the compound at room temperature (See SI for full characterization data). NMR data for **2**: ^{1}H NMR (600 MHz, CD_2Cl_2) δ 6.66 (d, J = 10.6 Hz, 4H), 6.06 (s, 4H), 3.67 (d, J = 10.7 Hz, 4H), 2.85 (s, 12H).

Synthesis of 3–6. Complexes **3**–**6** were synthesized by analogous routes, a representative synthesis for complex **3** is shown here (See SI for full synthetic procedures and characterization): In a glovebox, 25 mg of **L1** (1 equiv) and 32.7 mg Ni$(COD)_2$ (1 equiv) were suspended in 2 mL 2-chlorotoluene. The solution was allowed to stir for 16 hours at room temperature during which the solution color changed from yellow to murky brown. The solution was precipitated with pentane, filtered, and washed with pentane. The crude material was redissolved in CH_2Cl_2 and filtered over a pad of celite to remove Ni black. The CH_2Cl_2 solution was reduced to 1 mL, after which the product was precipitated with pentane. The isolated solid was filtered and washed with pentane to give 40 mg of the product as an orange solid in 85% yield. X-ray quality crystals were obtained by slow vapor diffusion of pentane into a THF solution of

© 2024 The Authors. ChemCatChem published by Wiley-VCH GmbH

the compound at −35 °C. NMR data for **3**: ^{1}H NMR (499 MHz, CD_2Cl_2) δ 7.27 (t, J = 7.8 Hz, 1H), 7.24–7.17 (m, 2H), 6.82 (d, J = 7.8 Hz, 2H), 6.78 (d, J = 7.8 Hz, 2H), 6.72 (d, J = 7.4 Hz, 1H), 6.62 (t, J = 7.4 Hz, 1H), 6.55 (t, J = 7.4 Hz, 1H), 6.23 (m, 4H), 3.77 (t, J = 10.5 Hz, 2H), 3.65 (t, J = 10.8 Hz, 2H), 3.30 (s, 3H); ^{13}C NMR (126 MHz, CD_2Cl_2) δ 160.15, 158.62, 146.14, 140.56, 138.73, 138.17, 136.97, 127.78, 123.57, 123.40, 122.91, 122.68, 36.21, 33.90, 26.14, 26.12.

NMR data for **4**: ^{1}H NMR (600 MHz, CD_2Cl_2) δ 7.26 (t, J = 7.7 Hz, 1H), 7.23 (t, J = 7.7 Hz, 1H), 7.08 (d, J = 8.0 Hz, 2H), 6.82 (d, J = 7.7 Hz, 2H), 6.79 (d, J = 7.7 Hz, 2H), 6.61 (d, J = 7.4 Hz, 2H), 6.15–6.03 (m, 4H), 3.78–3.70 (m, 2H), 3.66–3.59 (m, 2H), 2.14 (s, 3H); ^{13}C NMR (151 MHz, CD_2Cl_2) δ 159.88, 158.60, 138.70, 138.22, 138.16, 135.29, 132.19, 126.48, 123.34, 123.31, 36.17, 34.08, 20.61.

NMR data for **5**: ^{1}H NMR (600 MHz, CD_2Cl_2) δ 7.30 (d, J = 8.8 Hz, 1H), 6.66 (d, J = 7.4 Hz, 1H), 6.57 (t, J = 5.7 Hz, 1H), 6.52 (t, J = 6.4 Hz, 1H), 6.04 (m, 8H), 3.53–3.46 (m, 2H), 3.42–3.37 (m, 2H), 3.30 (s, 3H), 2.84 (s, 6H), 2.80 (s, 6H); ^{13}C NMR (151 MHz, CD_2Cl_2) δ 158.33, 157.50, 155.85, 155.48, 146.08, 137.33, 127.04, 122.14, 106.43, 105.90, 66.04, 39.47, 39.43, 36.21, 34.22, 26.15, 15.48.

NMR data for **6**: ^{1}H NMR (600 MHz, CD_2Cl_2) δ 7.09 (d, J = 7.8 Hz, 2H), 6.57 (s, 2H), 6.05 (s, 2H), 6.04 (s, 2H), 5.95–5.85 (m, 4H), 3.49–3.33 (m, 4H), 2.84 (s, 6H), 2.82 (s, 6H), 2.12 (s, 3H); ^{13}C NMR (151 MHz, CD_2Cl_2) δ 158.06, 157.44, 155.58, 138.46, 131.32, 125.93, 106.16, 105.91, 39.49, 39.47, 36.17, 34.38, 20.66.

Representative Cross-Coupling Catalytic Experiment. All reactions were done in the following conditions unless otherwise noted: a 2 M solution of *n*-octyl-MgCl (1.5 equiv, 0.15 mmol) was diluted to 0.5 mL with THF. The solution was then slowly added by the syringe pump over 1 h to a solution containing the catalyst (10 mol%, 0.01 mmol), 1.25 mL of THF and 0.25 mL of MeCN, and *n*-heptyl iodide (0.1 mmol) at room temperature. After the addition, the solution was stirred for an additional hour. It was then quenched by the addition of 2 mL of saturated NH_4Cl solution. *n*-Dodecane (22.7 μL, 0.1 mmol) was then added as an internal standard. The organic phase in the resulting solution mixture was extracted with 4 mL of ether and subjected to GC–FID analysis. All product yields were corrected with calibration curves and experimentally determined response factors, using dodecane as an internal standard.

Acknowledgements

We would like to acknowledge funding from the National Science Foundation (CHE-2155160 to L.M.M.). We would also like to thank Rachel Wallick for providing SQUID characterization for complex **1**, and Dr. Toby Woods and Dr. Danielle Gray for crystallographic assistance. We also thank all research facilities at the University of Illinois Urbana-Champaign.

Conflict of Interests

The authors declare no conflict of interest.

Data Availability Statement

Deposition Numbers 2311403-2311409 for **L2** and complexes **1**–**6** contain the supplementary crystallographic data for this paper. These data are provided free of charge by the joint Cambridge Crystallographic Data Centre and Fachinformationszentrum Karlsruhe Access Structures service.

Keywords: C–H bond activation · steric hindrance · cross coupling · nickel complexes

[1] a) J. Choi, G. C. Fu, *Science* **2017**, *356*, eaaf7230; b) J. B. Diccianni, T. Diao, *Trends Chem.* **2019**, *1*, 830–844; c) L.-C. Campeau, N. Hazari, *Organometallics* **2019**, *38*, 3–35.
[2] a) H. Xu, P. B. White, C. Hu, T. Diao, *Angew. Chem. Int. Ed.* **2017**, *56*, 1535–1538; b) Z. Lu, G. C. Fu, *Angew. Chem. Int. Ed.* **2010**, *49*, 6676–6678.
[3] a) C. Zhu, H. Yue, J. Jia, M. Rueping, *Angew. Chem. Int. Ed.* **2021**, *60*, 17810–17831; b) R. A. Escobar, J. W. Johannes, *Chem. Eur. J.* **2020**, *26*, 5168–5173.
[4] a) B. J. Shields, B. Kudisch, G. D. Scholes, A. G. Doyle, *J. Am. Chem. Soc.* **2018**, *140*, 3035–3039; b) S. I. Ting, S. Garakyaraghi, C. M. Taliaferro, B. J. Shields, G. D. Scholes, F. N. Castellano, A. G. Doyle, *J. Am. Chem. Soc.* **2020**, *142*, 5800–5810; c) H. Na, L. M. Mirica, *Nat. Commun.* **2022**, *13*, 1313; d) D. A. Cagan, D. Bim, B. Silva, N. P. Kazmierczak, B. J. McNicholas, R. G. Hadt, *J. Am. Chem. Soc.* **2022**, *144*, 6516–6531.
[5] a) S. Lou, G. C. Fu, *J. Am. Chem. Soc.* **2010**, *132*, 1264–1266; b) D. J. Weix, *Acc. Chem. Res.* **2015**, *48*, 1767–1775.
[6] a) B. Zheng, F. Tang, J. Luo, J. W. Schultz, N. P. Rath, L. M. Mirica, *J. Am. Chem. Soc.* **2014**, *136*, 6499–6504; b) F. Z. Tang, N. P. Rath, L. M. Mirica, *Chem. Commun.* **2015**, *51*, 3113–3116; c) J. W. Schultz, K. Fuchigami, B. Zheng, N. P. Rath, L. M. Mirica, *J. Am. Chem. Soc.* **2016**, *138*, 12928–12934; d) S. M. Smith, N. P. Rath, L. M. Mirica, *Organometallics* **2019**, *38*, 3602–3609; e) H. Na, M. B. Watson, F. Tang, N. Rath, L. M. Mirica, *Chem. Commun.* **2021**, *57*, 7264–7267.
[7] a) J. R. Khusnutdinova, N. P. Rath, L. M. Mirica, *Inorg. Chem.* **2014**, *53*, 13112–13129; b) A. J. Wessel, J. W. Schultz, F. Tang, H. Duan, L. M. Mirica, *Org. Biomol. Chem.* **2017**, *15*, 9923–9931.
[8] a) L. M. Mirica, J. R. Khusnutdinova, *Coord. Chem. Rev.* **2013**, *257*, 299–314; b) L. M. Mirica, S. M. Smith, L. Griego, in *Nickel Catalysis in Organic Synthesis* (Ed.: S. Ogoshi), Wiley-VCH, **2019**, pp. 223–248; c) N. Heberer, C.-H. Hu, L. M. Mirica, in *Comprehensive Coordination Chemistry III* (Eds.: E. C. Constable, G. Parkin, L. Que Jr.), Elsevier, Oxford, **2021**, pp. 348–374.
[9] H. Takemura, T. Shinmyozu, T. Inazu, *Tetrahedron Lett.* **1988**, *29*, 1031–1032.
[10] L. M. Mirica, H. Na, *U. S. Patent Application No.: 63/215,131, Filing date: June 25* **2021**.
[11] A. Okuniewski, D. Rosiak, J. Chojnacki, B. Becker, *Polyhedron* **2015**, *90*, 47–57.
[12] a) D. A. Evans, C. W. Downey, J. L. Hubbs, *J. Am. Chem. Soc.* **2003**, *125*, 8706–8707; b) W. J. Marshall, V. V. Grushin, *Can. J. Chem.* **2005**, *83*, 640–645.
[13] a) D. Lomjansky, C. Rajnák, J. Titis, J. Moncol, L. Smolko, R. Boca, *Inorg. Chim. Acta* **2018**, *483*, 352–358; b) H. D. Zheng, Y. W. Li, W. B. Du, C. S. Cheung, D. H. Li, H. Gao, H. Y. Deng, H. Y. Gao, *Macromolecules* **2022**, *55*, 3533–3540; c) H. Wang, W. Q. Lu, M. M. Zou, S. Y. Dai, *Molecules* **2023**, *28*, 2266.
[14] L. Falivene, Z. Cao, A. Petta, L. Serra, A. Poater, R. Oliva, V. Scarano, L. Cavallo, *Nat. Chem.* **2019**, *11*, 872–879.
[15] a) D. Braga, F. Grepioni, E. Tedesco, K. Biradha, G. R. Desiraju, *Organometallics* **1997**, *16*, 1846–1856; b) W. I. Sundquist, D. P. Bancroft, S. J. Lippard, *J. Am. Chem. Soc.* **1990**, *112*, 1590–1596.
[16] a) M. Brookhart, M. L. H. Green, G. Parkin, *Proc. Natl. Acad. Sci. USA* **2007**, *104*, 6908–6914; b) M. Brookhart, M. L. H. Green, *J. Organomet. Chem.* **1983**, *250*, 395–408; c) D. Braga, F. Grepioni, K. Biradha, G. R. Desiraju, *J. Chem. Soc. Dalton Trans.* **1996**, *25*, 3925–3930; d) Y. Zhang, J. C. Lewis, R. G. Bergman, J. A. Ellman, E. Oldfield, *Organometallics* **2006**, *25*, 3515–3519.
[17] R. Yadav, M. Trivedi, G. Kociok-Kohn, R. Prasad, A. Kumar, *CrystEngComm* **2015**, *17*, 9175–9184.
[18] M. P. Mitoraj, M. G. Babashkina, K. Robeyns, F. Sagan, D. W. Szczepanik, Y. V. Seredina, Y. Garcia, D. A. Safin, *Organometallics* **2019**, *38*, 1973–1981.
[19] G. C. Tucci, R. H. Holm, *J. Am. Chem. Soc.* **1995**, *117*, 6489–6496.
[20] N. Koga, S. Obara, K. Kitaura, K. Morokuma, *J. Am. Chem. Soc.* **1985**, *107*, 7109–7116.

© 2024 The Authors. ChemCatChem published by Wiley-VCH GmbH

18673899, 2024, 5, Downloaded from https://chemistry-europe.onlinelibrary.wiley.com/doi/10.1002/cctc.202301677 by University Of Illinois At, Wiley Online Library on [30/07/2024]. See the Terms and Conditions (https://onlinelibrary.wiley.com/terms-and-conditions) on Wiley Online Library for rules of use; OA articles are governed by the applicable Creative Commons License

[21] a) K. N. Zhing, M. Conda-Sheridan, S. R. Cooke, J. Louie, *Organometallics* **2011**, *30*, 2546–2552; b) S. I. Ting, W. L. Williams, A. G. Doyle, *J. Am. Chem. Soc.* **2022**, *144*, 5575–5582.
[22] a) L. Iffland, A. Petuker, M. Van Gastel, U.-P. Apfel, *Inorganics* **2017**, *5*, 78; b) S. L. Zultanski, G. C. Fu, *J. Am. Chem. Soc.* **2011**, *133*, 15362–15364.
[23] L. Griego, J. B. Chae, L. M. Mirica, *Chem* **2024**, *10*, 1–15, ASAP, https://doi.org/10.1016/j.chempr.2023.11.008.
[24] a) C. Wang, D. Wang, Z. S. Fu, Y. W. Qin, Q. S. Zhang, Z. Q. Fan, *J. Catal.* **2022**, *413*, 311–320; b) L. H. Guo, W. Q. Chen, W. J. Wang, W. Y. An, S. N. Gao, Y. Zhao, M. L. Luo, G. S. He, T. T. Liu, *J. Catal.* **2022**, *413*, 8–19.
[25] a) R. Kranthikumar, *Organometallics* **2022**, *41*, 667–679; b) H. Luo, Y. H. Feng, L. Q. Lin, *ChemCatChem* **2023**, *15*, e202300023.

Manuscript received: December 18, 2023
Revised manuscript received: January 20, 2024
Accepted manuscript online: January 24, 2024
Version of record online: February 8, 2024

© 2024 The Authors. ChemCatChem published by Wiley-VCH GmbH

18673899, 2024, 5, Downloaded from https://chemistry-europe.onlinelibrary.wiley.com/doi/10.1002/cctc.202301677 by University Of Illinois At, Wiley Online Library on [30/07/2024]. See the Terms and Conditions (https://onlinelibrary.wiley.com/terms-and-conditions) on Wiley Online Library for rules of use; OA articles are governed by the applicable Creative Commons License